Hindawi Publishing Corporation
Journal of Nanomaterials
Volume 2012, Article ID 983150, 7 pages
doi:10.1155/2012/983150

Research Article

Structural Studies and Optical and Electrical Properties of Novel Gd^{3+}-Doped Sb_2Se_3 Nanorods

Abdolali Alemi,[1] Younes Hanifehpour,[1,2] Sang Woo Joo,[2] Bong-Ki Min,[3] and Tae Hwan Oh[4]

[1] *Department of Inorganic Chemistry, Faculty of Chemistry, University of Tabriz, Tabriz 51664, Iran*
[2] *World Class University Nano Research Center, School of Mechanical Engineering, Yeungnam University, Gyongsan 712-749, Republic of Korea*
[3] *Center for Research Facilities, Yeungnam University, Gyongsan 712-749, Republic of Korea*
[4] *Department of Nano, Medical and Polymer Materials, Yeungnam University, Gyongsan 712-749, Republic of Korea*

Correspondence should be addressed to Abdolali Alemi, alemi.aa@gmail.com and Sang Woo Joo, swjoo@yu.ac.kr

Received 28 January 2012; Revised 17 March 2012; Accepted 14 May 2012

Academic Editor: Theodorian Borca-Tasciuc

Gd^{3+}-doped Sb_2Se_3 nanorods were synthesized by coreduction method at 180°C and pH = 12 for 48 h. Powder XRD patterns indicate that the $Gd_xSb_{2-x}Se_3$ crystals (x = 0.00–0.04) are isostructural with Sb_2Se_3. The cell parameters a and b increase for Gd^{3+} upon increasing the dopant content (x), while c decreases. SEM images show that doping of Gd^{3+} ions in the lattice of Sb_2Se_3 results in nanorods. High-resolution transmission electron microscopic (HRTEM) studies reveal that the $Gd_{0.04}Sb_{1.96}Se_3$ is oriented in the [10-1] growth direction. UV-Vis absorption reveals mainly electronic transitions of the Gd^{3+} ions in doped nanomaterials. Emission spectra of doped materials show sharp emission band originating from f-f transition $^6P_{7/2} \rightarrow {}^8S_{7/2}$ of the Gd^{3+} ions. The electrical conductance of Gd-doped Sb_2Se_3 is higher than undoped Sb_2Se_3 and increases with temperature.

1. Introduction

Investigations on semiconductor nanostructures have recently been in the focus of intensive research activities because of intrinsic fundamental interest and manifold possibilities for applications. Semiconductor selenides find applications as laser materials, optical filters, sensors, and solar cells. Antimony selenide, an important member of these V_2VI_3 compounds, is a layer-structured semiconductor of orthorhombic crystal structure, and exhibits good photovoltaic properties and high thermoelectric power (TEP) which allows possible applications for optical and thermoelectronic cooling devices [1–4]. Inorganic nanomaterials doped by lanthanide (Ln^{3+}) ions with various compositions have become an increasingly important research subject, and opened up opportunities for creating new applications in diverse fields, including biological labelling and imaging and light-emitting displays, owing to their distinct optical properties [5–7]. Over the past two decades, many methods have been employed to prepare Sb_2Se_3 nanotubes, nanowires, nanosheets, nanorods, nanobelts, nanospheres, and nanoflakes including thermal decomposition [8], microwave irradiation [1, 9], complex decomposition approach [10], solvothermal reaction [11–14], hydrothermal method [15, 16], vacuum evaporation [17], colloidal synthetic method [18], and other chemical reaction approaches. Studies of impurity effects or doping agents on the physical properties of Sb_2Se_3 are interesting both for basic and applied research. Doping of trivalent cations such as Sb^{3+} [19], In^{3+} [20], Fe^{3+} [21], Mn^{3+} [22], and a number of further trivalent 3d elements [23] to the lattice of Bi_2Se_3 has been investigated, also EPR spectra of Gd-doped bulk Bi_2Se_3 [24]. Also, new $Ln_xBi_{2-x}Se_3$ (Ln: Sm^{3+}, Eu^{3+}, Gd^{3+}, Tb^{3+}, Nd^{3+}) based nanomaterials were synthesized by Alemi et al. [25, 26]. Recently, we have reported novel luminescent nanomaterials based on doping of lanthanide (Ln: Ho^{3+}, Nd^{3+}, Lu^{3+}) into the lattice of Sb_2S_3 and (Ln: Ho^{3+}, Nd^{3+}, Lu^{3+}, Sm^{3+}, Er^{3+}, Yb^{3+}) into the lattice of Sb_2Se_3 [27–30]. The incorporation of large cations such as lanthanides into antimony chalcogenide frameworks is expected to lead to materials with different optical and electrical properties. The incorporation of lanthanide ions

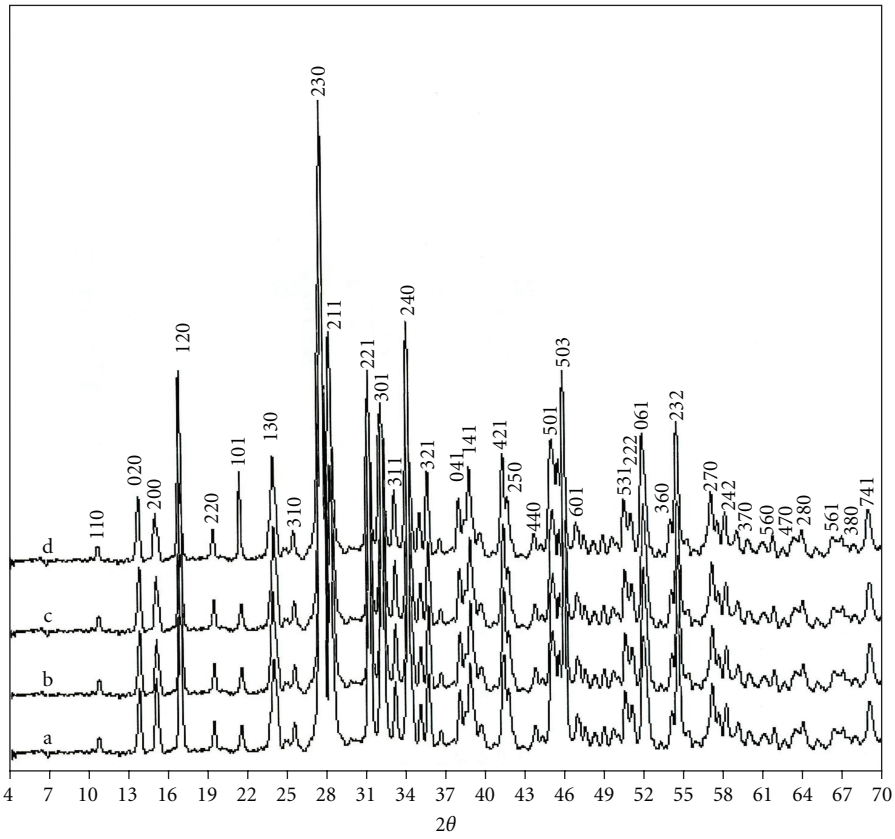

Figure 1: Powder X-ray diffraction patterns of $Sb_{2-x}Gd_xSe_3$ (a: $x = 0.0$, b: $x = 0.01$, c: $x = 0.02$, *d*: $x = 0.04$,) synthesized at 180°C and 48 h.

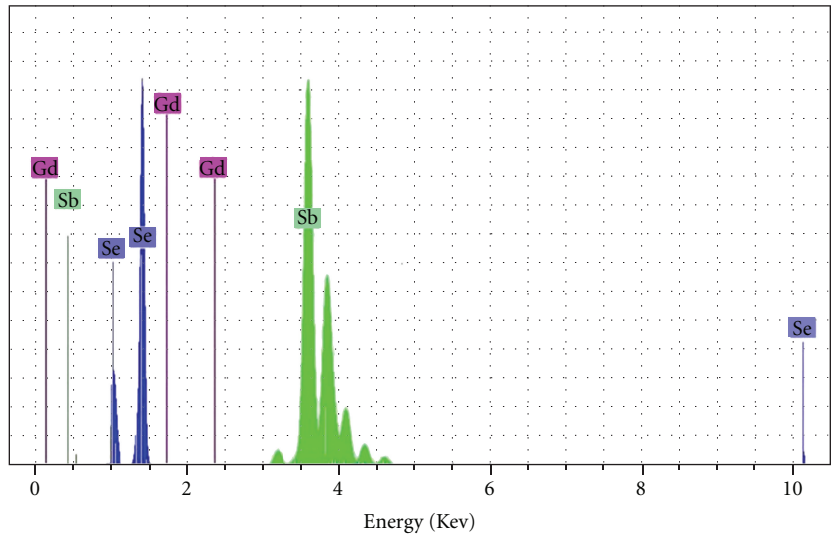

Figure 2: EDX patterns of $Sb_{1.96}Gd_{0.04}Se_3$ synthesized at 180°C and 48 h.

into a Sb–Se framework could dramatically affect the electronic properties of that framework. In this research, nanorods of $Gd_xSb_{2-x}Se_3$ crystals ($x = 0.00$–0.04) were synthesized by introducing small amounts of Gd^{3+} to the Sb_2Se_3 lattice. Structural, spectroscopic properties and electrical conductivity of the synthesized materials are reported.

2. Experiment

All chemicals were of analytical grade and were used without further purification. Grey selenium (1 mmol) and NaOH (5 mmol) were added to distilled water (60 mL) and stirred well for 10 min at room temperature. Afterwards,

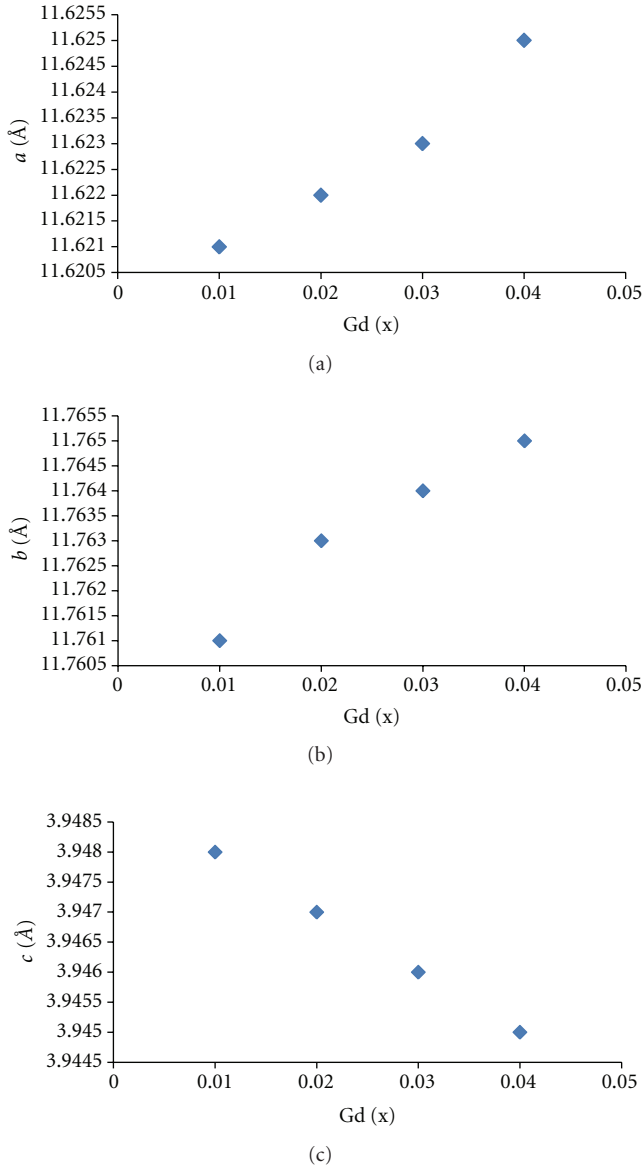

FIGURE 3: The lattice constant of $Sb_{2-x}Gd_xSe_3$ ($0 \leq x \leq 0.04$) dependent upon Gd^{3+} doping on Sb^{3+} sites.

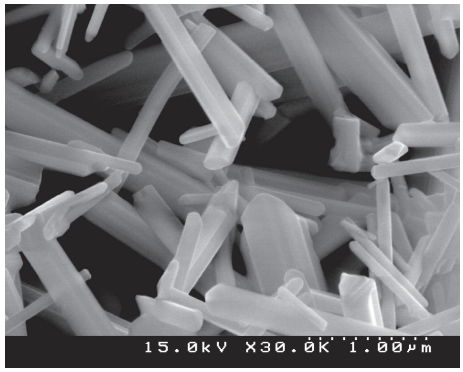

FIGURE 4: SEM image of Sb_2Se_3 nanorods synthesized at 180°C and 48 h.

hydrazinium hydroxide (2 mL, 40 mmol), $SbCl_3$ (2, 1.99, 1.98, 1.96 mmol) and Gd_2O_3 (0.00, 0.01, 0.02, 0.04 mmol) were added, and the mixture was transferred to a 100 mL Teflon-lined autoclave. The autoclave was sealed, maintained at 180°C for 48 h, and then cooled to room temperature. The optimum conditions for this reaction are pH = 12, temperature 180°C, and reaction time 48 h. The black precipitate obtained was filtered and washed with ethanol and water. It was dried at room temperature. Yields for the products were 85–90%. Phase identification was performed with an X-ray powder diffractometer (XRD D5000 Siemens) with Cu-K_α radiation. Cell parameters were calculated with Celref program from powder XRD patterns, and reflections have been determined and fitted using a profile fitting procedure with the Winxpow program. The reflections observed in 2θ = 4–70° were used for the lattice parameter determination. The morphology of materials were examined by a scanning electron microscope SEM (Hitachi S-4200). The HRTEM image and SAED pattern were recorded by a Cs-corrected high-resolution TEM (JEM-2200FS, JEOL) operated at 200 kV. Photoluminescence measurements were carried out using a Spex FluoroMax3 spectrometer after dispersing a trace amount of sample via ultrasound in distilled water. The Four-Probe Method was used for the measurement of electrical and thermoelectrical resistivity of samples. A small oven was needed for the variation of temperature of the samples from the room temperature to about 200°C (max.). Small chip with 1 mm thickness and 7 mm length was used for this analysis. This chip was obtained by pressing of 10 mg of sample under 30 kpa pressing device.

3. Results and Discussion

$Sb_{2-x}Gd_xSe_3$ samples were prepared by a hydrothermal coreduction method. $SbCl_3$ (99.99%), selenium powder, and Gd_2O_3 were used as starting materials, and hydrazinium hydroxide was used as the reducing agent. The powder X-ray diffraction (P-XRD) patterns (see. e.g. Figure 1) indicate that the Gd^{3+}-doped powders have the same orthorhombic structure as Sb_2Se_3 and that single phase Sb_2Se_3 is retained at lower doping concentrations of Gd^{3+}. All the peaks in the Figure 1 can be attributed to the orthorhombic phase of Sb_2Se_3 with pbnm space group and lattice parameters a = 11.62 Å, b = 11.76 Å, and c = 3.95 Å (JCPDS card File: 72-1184).

The EDX analysis of the product confirms the ratio of Sb/Se/Gd as expected (Figure 2). Also, ICP analysis confirms the exact amount of doping.

The cell parameters of the synthesized materials were calculated from the XRD patterns. With increasing dopant content (x), the a and b parameters for Gd^{3+} increase and the c decreases (Figure 3). The trend for lattice constants can be correlated to the effective ionic radii of the Gd^{3+} ions; assuming that the radius of Gd^{3+} is larger than that of Sb^{3+} results in greater amount of lattice parameters for Gd^{3+}-doped materials.

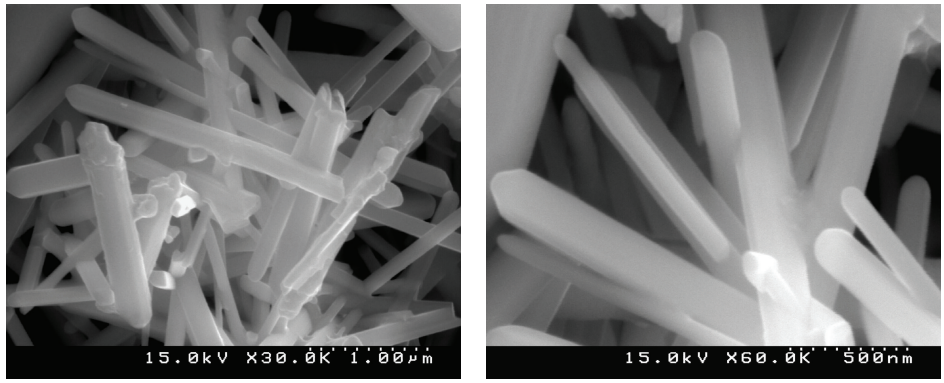

(a) (b)

Figure 5: SEM image of $Sb_{1.96}Gd_{0.04}Se_3$ nanorods (a) low and (b) high magnification synthesized at 180°C and 48 h.

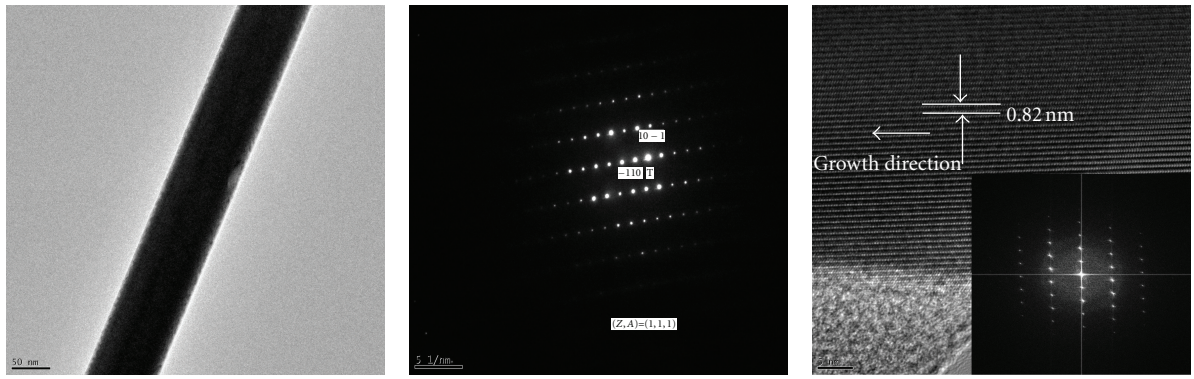

(a) (b) (c)

Figure 6: (a) TEM image (b) SAED of the $Sb_{1.96}Gd_{0.04}Se_3$ nanorods. The SAED zone axis is [10–1]. (c) HRTEM image and FFT pattern of the $Sb_{1.96}Gd_{0.04}Se_3$ nanorods.

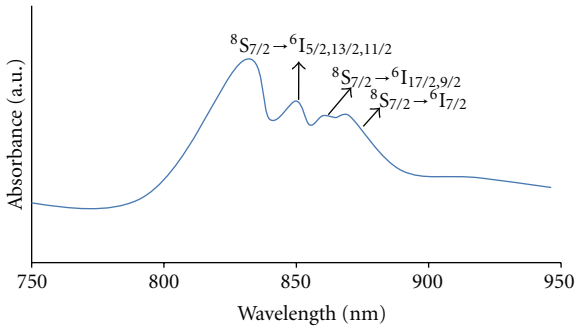

Figure 7: Absorption spectra of $Sb_{1.96}Gd_{0.04}Se_3$ at room temperature.

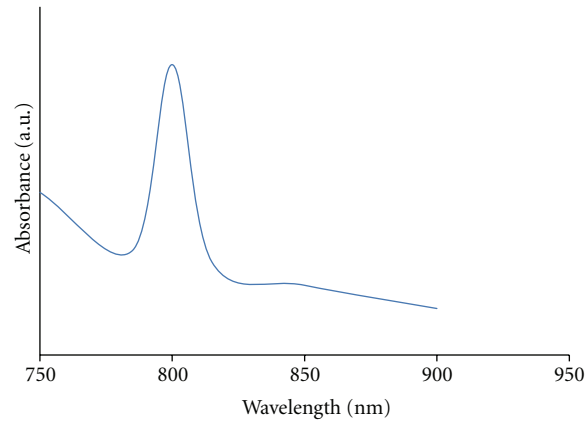

Figure 8: Absorption spectra of Sb_2Se_3 at room temperature.

Scanning electron microscopic (SEM) images of Sb_2Se_3 nanorods show rods up to 5 μm lengths and diameter of 25–120 nm (Figure 4).

Also, Figures 5(a) and 5(b) show SEM images of $Sb_{1.96}Gd_{0.04}Se_3$ nanorods in which the length of rods is about 6 μm lengths and diameters of 40–150 nm. Doping of Gd^{3+} into the structure of Sb_2Se_3 does not change the morphology of Sb_2Se_3 nanorods but the length and diameter of rods are changed.

Figure 6(a) shows TEM image of as-prepared $Sb_{1.96}Gd_{0.04}Se_3$ nanorods. The crystal lattice fringes are clearly observed and average distance between the neighboring fringes is 0.82 nm, corresponding to the [1–10] plane

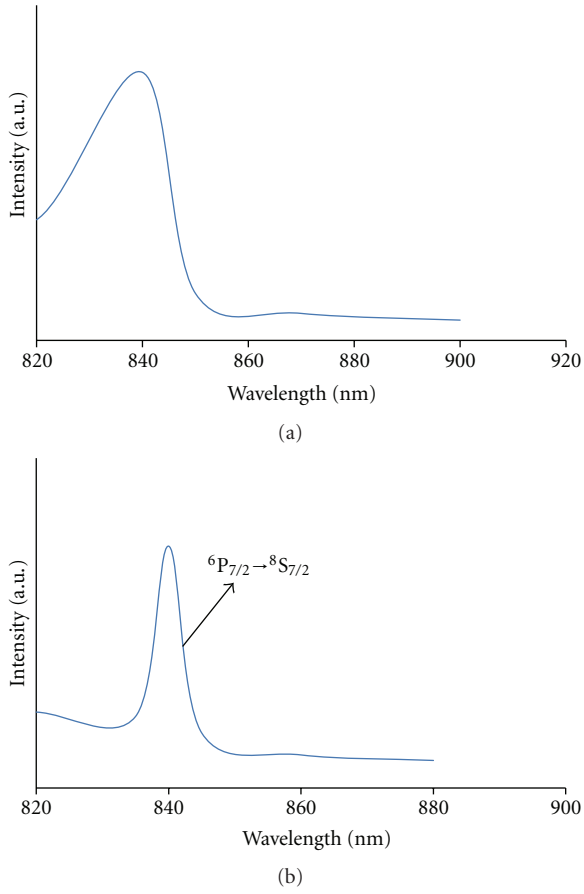

FIGURE 9: Excitation (a) and emission (b) spectra for Sb_2Se_3: Gd^{3+} at RT.

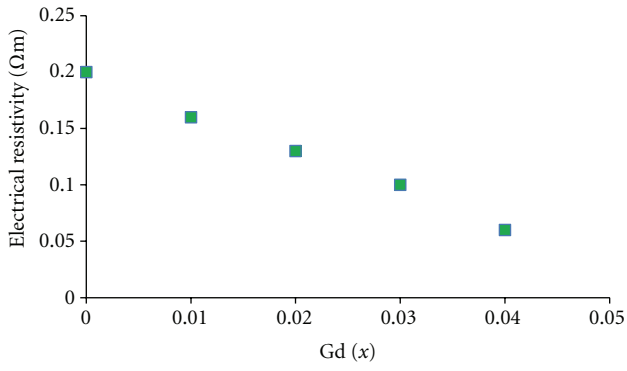

FIGURE 10: Electrical resistivity of $Sb_{1.96}Gd_{0.04}Se_3$ synthesized at 180°C and 48 h.

lattice distance of orthorhombic-structured Sb_2Se_3, which suggests that $Sb_{1.96}Gd_{0.04}Se_3$ nanorods grow along the [10–1] direction. The SAED pattern of the nanorods indicates its single crystal nature and long axis is [10–1] (Figure 6(b)). Also, the typical HRTEM image and FFT pattern recorded from the same nanorods are shown in Figure 6(c). The HRTEM image and SAED pattern are the same for Sb_2Se_3, and show the similar growth direction (see the Supplementary Material available online at doi:10.1155/2012/983150).

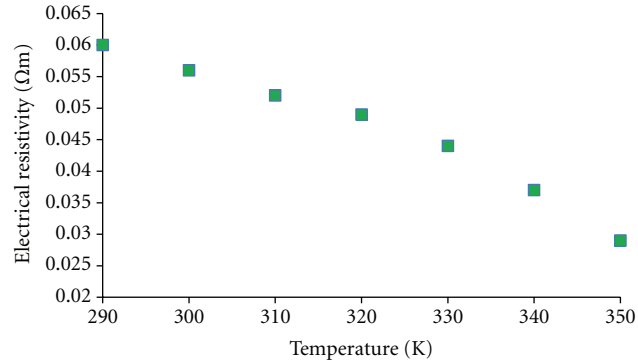

FIGURE 11: Thermoelectrical resistivity of $Sb_{1.96}Gd_{0.04}Se_3$ synthesized at 180°C and 48 h.

UV-Vis spectra of Gd^{3+} doped Sb_2Se_3 are shown in Figure 7. The absorption bands of Gd^{3+} doped Sb_2Se_3 exhibit maxima at 850, 860, and 870 nm were assigned to gadolinium electronic transition of $^8S_{7/2} \rightarrow {}^6I_{5/2,13/2,11/2}$, $^8S_{7/2} \rightarrow {}^6I_{17/2,\,9/2}$ and $^8S_{7/2} \rightarrow {}^6I_{7/2}$ [31, 32].

There is also a shift in the onset of absorption to lower energies (red shift) in Gd-doped samples compared to Sb_2Se_3 (see Figure 8). Band gap energies (E_g) for Sb_2Se_3 and $Sb_{1.96}Gd_{0.04}Se_3$ are calculated from the UV-Vis absorption spectra as $E_g = 1.55$ eV for pure Sb_2Se_3 and $E_g = 1.49$ eV for $Sb_{1.96}Gd_{0.04}Se_3$ [29, 30].

The sharp emission peak at 840 nm on excitation with the 835 nm in Figure 9 can be assigned to $^6P_{7/2} \rightarrow {}^8S_{7/2}$ transitions of Gd^{3+} [31, 32].

In doped semiconductors, the two types of emissions are responsible for the dopant (impurity) luminescence. One can be observed only upon direct excitation of the dopant. The second type is obtained if energy transfer from host to dopant occurs. Scheme 1 shows the band-gap model for the luminescence of Gd-doped Sb_2Se_3. The excitation of electrons across the host lattice band gap from the valence to conduction band is followed by a radiative recombination with a deeply trapped hole at a defect state or a nonradiative relaxation into the lanthanide ion 5d level. Radiative transition from the excited state to the ground state of Gd^{3+} ions occurs, leading to luminescence of the Gd^{3+} ions [26].

Binary compounds such as Sb_2Se_3 and its alloys are thermoelectric materials with layered crystalline structures. These materials have been investigated for direct conversion of thermal energy to electric energy and they specially are used for electronic refrigeration [33–36]. The Four-Probe Method was used for the measurement of electrical and thermoelectrical resistivity of samples (Scheme 2).

The electrical resistivity of the compounds is shown in Figure 10. With the increase in the lanthanide cation concentration, the electrical resistivity of synthesized nanomaterials decreased obviously. At room temperature the electrical resistivity of pure Sb_2Se_3 was of the order of $0.2\,\Omega \cdot m$ and for $Sb_{1.96}Gd_{0.04}Se_3$ was $6 \times 10^{-2}\,\Omega \cdot m$, respectively.

The temperature dependence of the electrical resistivity for $Sb_{1.96}Gd_{0.04}Se_3$ between 290–350 K is shown in Figure 11

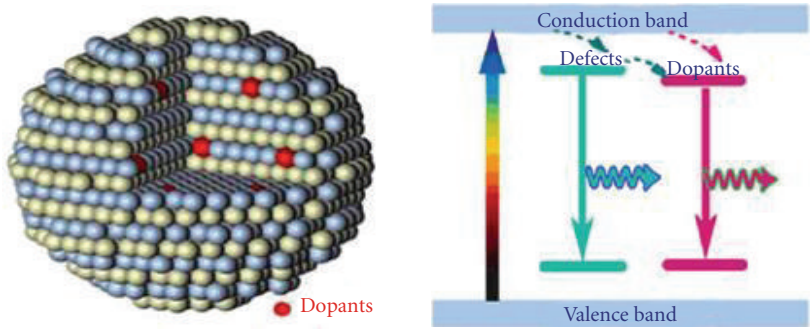

Scheme 1: Schematic bandgap model for the luminescence of Gd^{3+} doped in Sb_2Se_3.

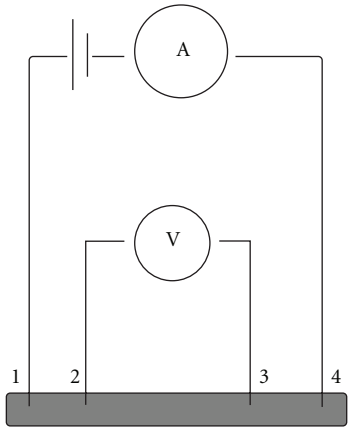

Scheme 2: Schematic of four-point probe.

in which electrical resistivity decreases with temperature. As a result, the electrical conductivity of Gd-doped Sb_2Se_3 materials is higher than pure Sb_2Se_3 at room temperature, and increases with temperature.

Two factors including overlapping of wavefunctions of electrons in doped Sb_2Se_3 and acting as a charge carrier due to Gd atomic structure (having empty f orbitals) are important reasons for decreasing electrical resistivity.

4. Conclusions

Coreduction synthesis is a simple and efficient method for preparing luminescent nanomaterials of $Gd_xSb_{2-x}Se_3$ (x = 0.00 to 0.04). SEM images show that doping of Gd^{3+} into the sites of the Sb^{3+} does not change the morphology of Sb_2Se_3. HRTEM images show that the growth direction is the same for pure Sb_2Se_3 and Gd-doped samples. Emission and absorption spectra of doped materials, in addition to the characteristic red emission peaks of Sb_2Se_3, show other emission bands originating from f-f transitions of the Gd^{3+} ions. The electrical conductivity of Gd-doped materials is higher than pure Sb_2Se_3 at room temperature, and increases with temperature.

Acknowledgment

This work is funded by the 2011 Yeungnam University Research Grant.

References

[1] C. Mastrovito, J. W. Lekse, and J. A. Aitken, "Rapid solid-state synthesis of binary group 15 chalcogenides using microwave irradiation," *Journal of Solid State Chemistry*, vol. 180, no. 11, pp. 3262–3270, 2007.

[2] S. K. Batabyal, C. Basu, G. S. Sanyal, and A. R. Das, "Synthesis of Sb_2Se_3 nanorod using β-cyclodextrin," *Materials Letters*, vol. 58, no. 1-2, pp. 169–171, 2004.

[3] X. Qiu, C. Burda, R. Fu, L. Pu, H. Chen, and J. Zhu, "Heterostructured Bi_2Se_3 nanowires with periodic phase boundaries," *Journal of the American Chemical Society*, vol. 126, no. 50, pp. 16276–16277, 2004.

[4] S. Subramanian and D. P. Padiyan, "Effect of structural, electrical and optical properties of electrodeposited bismuth selenide thin films in polyaniline aqueous medium," *Materials Chemistry and Physics*, vol. 107, no. 2-3, pp. 392–398, 2008.

[5] F. Wang, Y. Han, C. S. Lim et al., "Simultaneous phase and size control of upconversion nanocrystals through lanthanide doping," *Nature*, vol. 463, no. 7284, pp. 1061–1065, 2010.

[6] T. Tachikawa, T. Ishigaki, J. G. Li, M. Fujitsuka, and T. Majima, "Defect-mediated photoluminescence dynamics of Eu^{3+}-doped TiO_2 nanocrystals revealed at the single-particle or single-aggregate level," *Angewandte Chemie—International Edition*, vol. 47, no. 29, pp. 5348–5352, 2008.

[7] Y. Jiang, Y. J. Zhu, and G. F. Cheng, "Synthesis of Bi_2Se_3 nanosheets by microwave heating using an ionic liquid," *Crystal Growth and Design*, vol. 6, no. 9, pp. 2174–2176, 2006.

[8] S. Messina, M. T. S. Nair, and P. K. Nair, "Solar cells with Sb_2S_3 absorber films," *Thin Solid Films*, vol. 517, no. 7, pp. 2503–2507, 2009.

[9] C. Zhao, X. Cao, and X. Lan, "Microwave-enhanced rapid and green synthesis of well crystalline Sb_2Se_3 nanorods with a flat cross section," *Materials Letters*, vol. 61, no. 29, pp. 5083–5086, 2007.

[10] M. Lalia-Kantouri and G. E. Manoussakis, "Thermal decomposition of tris(*N, N*-disubstituted dithiocarbamate) complexes of As(III), Sb(III) and Bi(III)," *Journal of Thermal Analysis*, vol. 29, no. 5, pp. 1151–1169, 1984.

[11] J. Yang, J. H. Zeng, S. H. Yu, L. Yang, Y. H. Zhang, and Y. T. Qian, "Pressure-controlled fabrication of stibnite nanorods

by the solvothermal decomposition of a simple single-source precursor," *Chemistry of Materials*, vol. 12, no. 10, pp. 2924–2929, 2000.

[12] W. J. Lou, M. Chen, X. B. Wang, and W. M. Liu, "Novel single-source precursors approach to prepare highly uniform Bi_2S_3 and Sb_2S_3 nanorods via a solvothermal treatment," *Chemistry of Materials*, vol. 19, no. 4, pp. 872–878, 2007.

[13] D. Wang, D. Yu, M. Mo, X. Liu, and Y. Qian, "Preparation and characterization of wire-like Sb_2Se_3 and flake-like Bi_2Se_3 nanocrystals," *Journal of Crystal Growth*, vol. 253, no. 1-4, pp. 445–451, 2003.

[14] J. Lu, Q. Han, X. Yang, L. Lu, and X. Wang, "Preparation of ultra-long Sb_2Se_3 nanoribbons via a short-time solvothermal process," *Materials Letters*, vol. 62, no. 16, pp. 2415–2418, 2008.

[15] D. Wang, D. Yu, M. Shao, J. Xing, and Y. Qian, "Growth of Sb_2Se_3 whiskers via a hydrothermal method," *Materials Chemistry and Physics*, vol. 82, no. 3, pp. 546–550, 2003.

[16] Q. Xie, Z. Liu, M. Shao, L. Kong, W. Yu, and Y. Qian, "Polymer-controlled growth of Sb_2Se_3 nanoribbons via a hydrothermal process," *Journal of Crystal Growth*, vol. 252, no. 4, pp. 570–574, 2003.

[17] O. Savadogo and K. C. Mandal, "Studies on new chemically deposited photoconducting antimony trisulphide thin films," *Solar Energy Materials and Solar Cells*, vol. 26, no. 1-2, pp. 117–136, 1992.

[18] Z. Deng, M. Mansuripur, and A. J. Muscat, "Simple colloidal synthesis of single-crystal Sb–Se–S nanotubes with composition dependent band-gap energy in the near-infrared," *Nano Letters*, vol. 9, no. 5, pp. 2015–2020, 2009.

[19] N. S. Patil, A. M. Sargar, S. R. Mane, and P. N. Bhosale, "Growth mechanism and characterisation of chemically grown Sb doped Bi_2Se_3 thin films," *Applied Surface Science*, vol. 254, no. 16, pp. 5261–5265, 2008.

[20] S. Augustine and E. Mathai, "Growth, morphology, and microindentation analysis of Bi_2Se_3, $Bi_{1.8}In_{0.2}Se_3$, and $Bi_2Se_{2.8}Te_{0.2}$ single crystals," *Materials Research Bulletin*, vol. 36, no. 13-14, pp. 2251–2261, 2001.

[21] P. Lostak, C. Drasar, I. Klichova, J. Navratil, and T. Cernohorsky, "Properties of Bi_2Se_3 single crystals doped with Fe atoms," *Physica Status Solidi B*, vol. 200, no. 1, pp. 289–296, 1997.

[22] P. Janícek, C. Drasar, P. Lostákand, J. Vejpravová, and V. Sechovský, "Transport, magnetic, optical and thermodynamic properties of $Bi_{2-x}Mn_xSe_3$ single crystals," *Physica B*, vol. 403, no. 19-20, pp. 3553–3558, 2008.

[23] P. Larson and W. R. L. Lambrecht, "Electronic structure and magnetism in Bi_2Te_3, Bi_2Se_3, and Sb_2Te_3 doped with transition metals (Ti–Zn)," *Physical Review B* , vol. 78, no. 19, Article ID 195207, 2008.

[24] X. Gratens, S. Isber, S. Charar et al., "EPR study of fine and hyperfine interactions of Gd^{3+} in $Bi_{2(1-x)}Gd_{2x}Se_3$ and $Pb_{1-x}Gd_xSe$," *Physical Review B*, vol. 55, no. 13, pp. 8075–8078, 1997.

[25] A. Alemi, A. Babalou, M. Dolatyari, A. Klein, and G. Meyer, "Hydrothermal synthesis of NdIII doped Bi_2Se_3 nanoflowers and their physical properties," *Zeitschrift für Anorganische und Allgemeine Chemie*, vol. 635, no. 12, pp. 2053–2057, 2009.

[26] A. Alemi, A. Klein, G. Meyer, M. Dolatyari, and A. Babalou, "Synthesis of new $Ln_xBi_{2-x}Se_3$ (Ln: Sm^{3+}, Eu^{3+}, Gd^{3+}, Tb^{3+}) nanomaterials and investigation of their optical properties," *Zeitschrift für Anorganische und Allgemeine Chemie*, vol. 637, no. 1, pp. 87–93, 2011.

[27] A. Alemi, Y. Hanifehpour, S. W. Joo, A. Khandar, A. Morsali, and B. K. Min, "Co-reduction synthesis of new $Ln_xSb_{2-x}S_3$ (Ln: Nd^{3+}, Lu^{3+}, Ho^{3+}) nanomaterials and investigation of their physical properties," *Physica B*, vol. 406, no. 14, pp. 2801–2806, 2011.

[28] A. Alemi, Y. Hanifehpour, S. W. Joo, and B. K. Min, "Structural studies and physical properties of novel Sm^{3+}-doped Sb_2Se_3 nanorods," *Physica B*, vol. 406, no. 20, pp. 3831–3835, 2011.

[29] A. Alemi, Y. Hanifehpour, S. W. Joo, A. Khandar, A. Morsali, and B. Min, "Synthesis and characterization of new $Ln_xSb_{2-x}Se_3$ (Ln: Yb^{3+}, Er^{3+}) nanoflowers and their physical properties," *Physica B*, vol. 407, no. 1, pp. 38–43, 2012.

[30] A. Alemi, Y. Hanifehpour, S. W. Joo, and B. Min, "Synthesis of novel $Ln_xSb_{2-x}Se_3$ (Ln: Lu^{3+}, Ho^{3+}, Nd^{3+}) nanomaterials via co-reduction method and investigation of their physical properties," *Colloids and Surfaces A*, vol. 390, no. 1–3, pp. 142–148, 2011.

[31] K. Binnemans and C. Görller-Walrand, "On the color of the trivalent lanthanide ions," *Chemical Physics Letters*, vol. 235, no. 3-4, pp. 163–174, 1995.

[32] R. C. Ropp, "Phosphors based on rare earth phosphates," *Journal of the Electrochemical Society*, vol. 115, no. 8, pp. 841–845, 1968.

[33] T. S. Kim and B. S. Chun, "Microstructure and thermoelectric properties of n- and p-type Bi_2Te_3 alloys by rapid solidification processes," *Journal of Alloys and Compounds*, vol. 437, no. 1-2, pp. 225–230, 2007.

[34] X. H. Ji, X. B. Zhao, Y. H. Zhang, B. H. Lu, and H. L. Ni, "Solvothermal synthesis and thermoelectric properties of lanthanum contained Bi–Te and Bi–Se–Te alloys," *Materials Letters*, vol. 59, no. 6, pp. 682–685, 2005.

[35] R. J. Mehta, C. Karthik, W. Jiang et al., "High electrical conductivity antimony selenide nanocrystals and assemblies," *Nano Letters*, vol. 10, no. 11, pp. 4417–4422, 2010.

[36] R. B. Yang, J. Bachmann, E. Pippel et al., "Pulsed vapor-liquid-solid growth of antimony selenide and antimony sulfide nanowires," *Advanced Materials*, vol. 21, no. 31, pp. 3170–3174, 2009.